J|A|C|S
ARTICLES
Published on Web 04/03/2004

Widely-Applicable Gold Substrate for the Study of Ultrathin Overlayers

Meni Wanunu, Alexander Vaskevich, and Israel Rubinstein*

Contribution from the Department of Materials and Interfaces, Weizmann Institute of Science, Rehovot 76100, Israel

Received November 17, 2003; E-mail: israel.rubinstein@weizmann.ac.il

Abstract: Ultrathin films on gold substrates have been the subject of enormous scientific and technological interest. Comprehensive study of such systems requires concomitant application of a variety of complementary characterization techniques. The reliability of the result is frequently hampered by the fact that different characterization methods impose different requirements on the Au substrate, resulting in the need to use different types of Au substrates for different measurements, possibly influencing the overlayer structure. This results in an average, rather than exact, structure determination. Here, we show that 15-nm-thick Au films evaporated at 0.5 Å/sec on silanized glass and annealed are semi-transparent, electrically conducting, and morphologically well-defined, showing a smooth, {111} textured surface. Such Au films provide a high-quality, widely applicable and relatively inexpensive platform for ultrathin overlayers, enabling characterization by a wide spectrum of experimental methods, applied to the same substrate. The exceptional qualities and analytical capabilities of such substrates are demonstrated with several different systems: (i) Cu underpotential deposition (upd); (ii) alkanethiol self-assembly; (iii) formation of Au nanoparticle layers; (iv) binding of the chromophore protoporphyrin IX (PPIX) to a monolayer of 11-mercaptoundecanoic acid (MUA). In the latter case it is shown that the use of Cu^{2+} ions for binding between the carboxylate groups of PPIX and MUA promotes better organization of the porphyrin layer.

Introduction

Preparation of ultrathin overlayers, such as self-assembled monolayers (SAMs),[1,2] on gold surfaces, has been a major area of research in recent years. As a consequence, a multitude of techniques for the investigation of ultrathin layers on Au have been developed, enabling detection and characterization of adsorbed layers in the (sub) monolayer range. Due to the limitations of any single characterization method, a number of measurements using independent techniques are required to fully characterize such layers. Accordingly, the Au substrates used must be suitable for each of the characterization techniques applied. This, however, is not always accomplished with a single kind of Au substrate. For example, while ellipsometric measurements of SAMs are usually performed using thick (typically 100−300 nm), reflective Au films evaporated on flat substrates (e.g., highly polished Si),[3] transmission spectroscopy of SAMs requires ultrathin Au films deposited on transparent substrates.[4] The characterization is then complicated by the fact that there may be differences in the structure of the SAM on the different types of Au surfaces. It is therefore highly desirable to develop a simple, high-quality and reproducible Au substrate that can accommodate a large variety of independent characterization techniques.

Optically transparent Au films can be produced by evaporation of several nanometers of Au on transparent substrates (e.g., glass, mica). At thicknesses somewhat above the percolation threshold (ca. 5−10 nm, depending on the substrate and the evaporation conditions), Au films become conductive while remaining semi-transparent, enabling their use in electrochemical as well as in transmission spectroscopy experiments.[5] Whitesides and co-workers[4] used transparent Au films on glass to study the adsorption of a chromophore-labeled protein onto alkanethiol SAMs. Murray and co-workers[6] used transparent Au films for the detection of thiol-derivatized porphyrin monolayers. Hatton et al.[7] prepared 7 nm transparent Au films on silanized glass for LED application.

Ellipsometry, a major technique providing invaluable information on the thickness and optical properties of ultrathin layers on Au substrates,[2,3] is usually considered incompatible with transmission spectroscopy, as it requires reflective surfaces. Hence, thick (100−300 nm) evaporated Au films are commonly used for ellipsometric studies of SAMs. However, at the high angles of incidence used in ellipsometry (typically $\phi = 70°$),

(1) Nuzzo, R. G.; Allara, D. L. *J. Am. Chem. Soc.* **1983**, *105*, 4481−4483.
(2) Ulman, A. *An Introduction to Ultrathin Organic Films*; Academic Press: Boston, 1991.
(3) Finklea, H. O. In *Electroanalytical Chemistry: A Series of Advances*; Bard, A. J., Rubinstein, I., Eds.; Marcel Dekker: New York, 1996; Vol. 19, pp 136−138.
(4) DiMilla, P. A.; Folkers, J. P.; Biebuyck, H. A.; Harter, R.; Lopez, G. P.; Whitesides, G. M. *J. Am. Chem. Soc.* **1994**, *116*, 2225−2226.
(5) See e.g., I. Ruach-Nir, Ph.D. Dissertation, Weizmann Institute of Science, 2003, Section 3.2.3.
(6) Postlethwaite, T. A.; Hutchison, J. E.; Hathcock, K. W.; Murray, R. W. *Langmuir* **1995**, *11*, 4109−4116.
(7) Hatton, R. A.; Willis, M. R.; Chester, M. A.; Briggs, D. *J. Mater. Chem.* **2003**, *13*, 722−726.

10.1021/ja0396448 CCC: $27.50

thin, transparent Au films may be reflective enough for ellipsometry, pointing to the attractive possibility of concurrent application of transmission spectroscopy, ellipsometry and electrochemistry using the same Au substrates.

In this work, semi-transparent, continuous, 15-nm-thick Au films evaporated on aminosilane-treated glass slides and subsequently annealed, are shown to be exceptionally suitable for the study of ultrathin overlayers, providing a high-quality, {111} textured Au surface as well as a universal platform for the application of a large variety of characterization methods. The superior applicability of these substrates was demonstrated in the following manner: The semi-transparent Au substrates were first characterized by X-ray diffraction (XRD), transmission electron microscopy (TEM), high-resolution scanning electron microscopy (HRSEM), atomic force microscopy (AFM), and electrochemical methods. Then, alkanethiol monolayers of varying chain length were assembled on these substrates and analyzed by ellipsometry, contact angle (CA) measurements and FTIR spectroscopy. Binding of Au nanoparticles (NPs) to thiol-terminated SAMs was then followed by transmission UV−vis spectroscopy and AFM imaging. Finally, the stepwise binding of protoporphyrin IX (PPIX) to carboxylate or to carboxylate/metal ion terminated functional SAMs was monitored by transmission spectroscopy, ellipsometry, CA measurements, and X-ray photoelectron spectroscopy (XPS). For comparison, similar experiments (excluding transmission spectroscopy) were carried out on thick (100 nm) Au films.

Experimental Section

Chemicals and Materials. Methanol (AR, Baker), Ethanol (AR, Merck), H_2SO_4 (95−98%, Palacid, Israel and 98% extra pure, Merck), NH_3 (25%, Frutarom, Israel), H_2O_2 (30%, Frutarom), 3-aminopropyl trimethoxysilane (APTMS) (97%, Aldrich), $CuSO_4 \cdot 5H_2O$ (>99.0%, Merck), 11-mercaptoundecanoic acid (MUA) (95%, Aldrich), $Cu(ClO_4)_2 \cdot 6H_2O$ (>98%, Fluka), 1,10-decanedithiol (97%, Lancaster) and protoporphyrin IX (PPIX) (>90%, Aldrich) were used as received. 1-octanethiol (98.5+%, Aldrich) and 1-dodecanethiol (98+%, Aldrich) were distilled under vacuum. 1-octadecanethiol (98%, Aldrich) was recrystallized from ethanol. Water was triply distilled. Samples were dried using household N_2 (>99%). Au (99.99%, Holland-Moran, Israel) was used for evaporated Au films. Substrates were prepared from Si wafers (p-type, polished, ⟨111⟩ orientation, International Wafer Service, USA) or glass, either thin (0.3 mm thick, microscope cover slips #3, Marienfield, Germany) or thick (1 mm thick, precleaned microscope slides, Chase Scientific Glass), cut to 1.0 × 2.0 cm pieces. Thin glass substrates were used except when specified otherwise.

Silanization of Substrates. Si and glass substrates were derivatized as follows:[8] The substrates were first cleaned with piranha solution (*caution: Pirahna solution reacts violently with organic materials and should be handled with extreme care*) for 20 min, then treated with 1:1:2 H_2O_2:NH_3:H_2O at 70 °C for 20 min, followed by copious rinsing with water and methanol. The substrates were then shaken in a 10% solution of APTMS in methanol for 3 h, rinsed and sonicated in methanol, and dried under a N_2 stream.

Preparation of Au Films. Au films were prepared by resistive evaporation in a cryo-HV evaporator (Key High Vacuum) equipped with a Maxtek TM-100 thickness monitor. Au (99.99%) was evaporated from a tungsten boat at 1−5 μTorr at a deposition rate of 1.0 Å/sec and 0.5 Å/sec for Si and glass substrates, respectively. Au films (100 nm) on Si were annealed (220 °C, 20 h) in air. Au films (15.0 nm) on glass were either used directly or annealed (200 °C, 20 h). All Au substrates were cleaned immediately before use by UV/ozone (UVOCS T10 × 10/OES/E system) for 10 min followed by immersion in stirred ethanol for 20 min.[9]

Scheme 1. Schematic Illustration of the Stepwise Construction of a Protoporphyrin IX (PPIX) Monolayers on Carboxylate-terminated MUA SAMs Either with (A) or without (B) a Cu^{2+} Binding Step

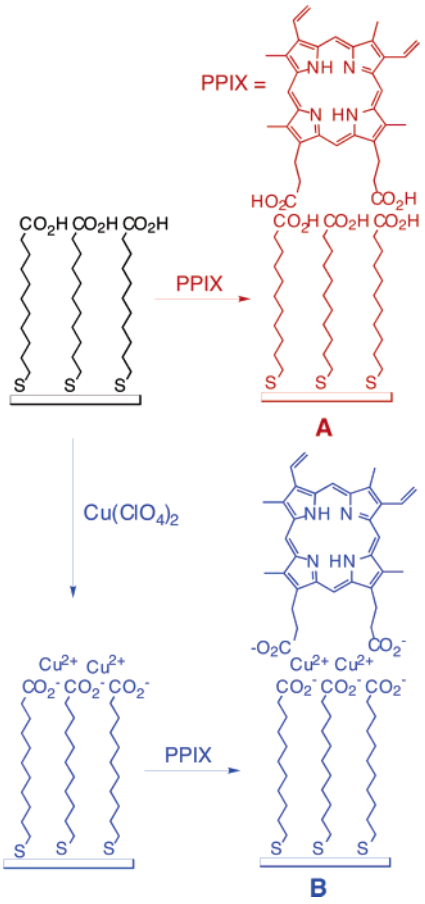

Preparation of Thiol SAMs. Monolayers were prepared by immersion of the substrates in ethanolic solutions of the different thiols. The concentrations were 10 mM (octanethiol, dodecanethiol) and 1 mM (octadecanethiol, 1,10-decanedithiol, MUA). Immersion times were 4 h for 1,10-decanedithiol and overnight for all other thiols.

Binding of Au Nanoparticles (NPs) to Thiol-Terminated Au Substrates. Two types of Au NPs were prepared, using the phase-transfer agent tetraoctylammonium bromide (TOAB), following the procedure of Brust et al.[10] Two types of Au NPs were prepared: (i) using octanethiol as the stabilizing shell (2.6 ± 0.6 nm diameter); (ii) using TOAB as the stabilizing shell (5.2 ± 1.2 nm diameter). Both types of NPs were bound to Au surfaces modified with 1,10-decanedithiol. For NP binding, the substrates were immersed in the respective NP solutions overnight.

Formation of PPIX SAMs. Scheme 1 illustrates the construction of PPIX monolayers. PPIX was bound to SAMs of MUA either with (**A**) or without (**B**) a layer of bound Cu^{2+} ions. Cu^{2+} was bound to MUA SAMs by immersion in a 10 mM solution of $Cu(ClO_4)_2$ in ethanol for 10 min,[11] followed by rinsing with ethanol. PPIX was bound by immersion in a 0.2 mM solution of PPIX in ethanol for 6−10 h, followed by rinsing with ethanol.

Atomic Force Microscopy (AFM). Tapping-mode AFM measurements were carried out in air, using a PicoSPM (Molecular Imaging,

(8) Grabar, K. C.; Freeman, R. G.; Hommer, M. B.; Natan, M. J. *Anal. Chem.* **1995**, *67*, 735−743.
(9) Ron, H.; Matlis, S.; Rubinstein, I. *Langmuir* **1998**, *14*, 1116−1121.
(10) Brust, M.; Bethell, D.; Schiffrin, D. J.; Kiely, C. *J. Adv. Mater* **1995**, *7*, 795−797.
(11) Zamborini, F. P.; Leopold, M. C.; Hicks, J. F.; Kulesza, P. J.; Malik, M. A.; Murray, R. W. *J. Am. Chem. Soc.* **2002**, *124*, 8958−8964.

USA) instrument. The tips used in all measurements were NSC12 (MikroMasch, Estonia) at a resonant frequency of ca. 100 kHz.

High-Resolution Scanning Electron Microscopy (HRSEM). HRSEM imaging was carried out with a JEOL JSM-6700F microscope (Tel-Aviv University). All images were scanned with a 2 kV beam voltage and detected using the secondary electron detector, at a magnification of 150 000×.

Transmission Electron Microscopy (TEM). TEM bright-field imaging and electron diffraction were carried out with a Philips CM-120 microscope operating at 120 kV. For TEM measurements, free-standing Au substrates were prepared by floating the Au films on the surface of a 5% aqueous HF solution.[12] The films were lifted onto a TEM copper grid and dried under an incandescent lamp for 1 h. Electron diffraction was taken from a spot of ca. 80 nm diameter in the center of the image.

X-Ray Diffraction (XRD). XRD measurements were carried out using a Rigaku RU-200B Rotaflex powder diffractometer operated in the θ-2θ Bragg configuration using Cu (Kα) radiation. The voltage was set to 50 kV with a flux of 150 mA. Data for $\theta-2\theta$ experiments were collected in the range from 30° to 79°, using a scan rate of 0.5° min^{-1} and a sampling interval of 0.05°.

Transmission UV−Vis Spectroscopy. Transmission spectra were obtained with a Varian Cary 50 UV−vis spectrophotometer. All measurements were carried out in air, using a homemade holder designed for reproducibility of the sampled spot. Spectra were recorded in the range 300−700 nm using air as baseline.

Electrochemical Measurements. Electrochemical experiments were conducted with an EG&G PARC 263A potentiostat controlled by Model 270/250 Research Electrochemical Software (Princeton Applied Research, USA). Cyclic voltammetry (CV) experiments were carried out in a single-compartment three-electrode cell with a K_2SO_4-saturated mercurous sulfate reference electrode (MSE) and a Pt foil counter electrode. The supporting electrolyte was aqueous 0.1 M H_2SO_4. The geometric area of the Au substrate was 0.33 cm^2, controlled by a 0.25" O-ring. Cu underpotential deposition (upd) was carried out in a solution containing 1.0 mM $CuSO_4$ in 0.1 M H_2SO_4. To test the stability of the Au films, 10 consecutive voltammograms (in 0.1 M H_2SO_4) were performed with each substrate in the Au oxidation/reduction region (0.0−1.0 V vs MSE) after each electrochemical experiment. The films remained intact in all cases. *Note that the stability of octanethiol-coated Au films toward electrochemical treatment in aqueous solutions is poor when the slide edges are exposed to the solution, resulting in Au detachment. This problem can be avoided by confining the exposed electrode area, as done in the present case using an O-ring.*

Ellipsometry. Ellipsometric measurements were carried out with a Rudolph Research Auto-EL IV null ellipsometer, at an angle of incidence $\phi = 70°$ and a wavelength $\lambda = 632.8$ nm. The same four points were measured on each sample before and after self-assembly. Film thickness was calculated using a film refractive index of $n_f = 1.50$, $k_f = 0$.

Contact Angle (CA) Measurements. Advancing and receding water CAs were measured using a computerized CA meter (KSV Instruments, Finland). Data collection and analysis were carried out using the provided CAM100 software. CAs were measured on three different spots in each sample.

Reflection−Absorption FTIR (RA-FTIR) Spectroscopy. FTIR spectra were recorded with a N_2-purged Bruker Equinox 55 spectrometer operating in the reflection mode (80° incidence angle), equipped with a MCT detector. Data were collected at a resolution of 2 cm^{-1}, and 1024 consecutive scans were taken for both background and sample. The background was prepared by exposing an Au substrate to UV/ozone + ethanol dip treatment (see above, Preparation of Au films), followed by a second 5 min UV/ozone treatment, immediately before measurement.

X-Ray Photoelectron Spectroscopy (XPS). XPS measurements were carried out with a Kratos Axis HS XPS system, using monochromatized Al (Kα) X-ray source ($h\nu = 1486.6$ eV). To minimize beam-induced damage, a low dose was maintained, using a relatively low beam flux (5 mA emission current at 15 keV) and medium energy resolution (pass energy of 80 eV). Angle-resolved XPS measurements were performed at takeoff angles of 90° and 25°.

Results and Discussion

Characterization of the Au Substrates. Three types of Au substrates were studied: (i) 100 nm annealed Au films on Si (denoted substrate **I**); (ii) 15 nm unannealed Au films on glass (denoted substrate **II**); and (iii) 15 nm annealed Au films on glass (denoted substrate **III**). In all cases, except the FTIR measurements (see below), substrates **II** and **III** were prepared using the thin glass slides (see Experimental Section). To improve the adhesion of the evaporated gold, the substrates were derivatized with a monolayer of APTMS prior to Au deposition.

AFM and HRSEM imaging were used to investigate the morphology of the Au films. All three substrates exhibit a continuous grain structure, characteristic of evaporated Au films (Figure 1). However, the average grain dimensions and the overall surface roughness differ between substrates. While the unannealed film **II** exhibits a uniform structure with small grains and random voids (Figure 1b,e), the annealed films **I** (Figure 1a,d) and **III** (Figure 1c,f) exhibit large, flat domains and are essentially void-free. Note that the annealed 15 nm substrate **III** is smoother than the annealed 100 nm substrate **I** (see z-scale in Figure 1), with both substrates showing grains of the order of several hundred nm. Analysis of the rms roughness in the AFM images results in the values 11.5, 18.9, and 7.8 Å (±1.5 Å) for substrates **I**, **II**, and **III**, respectively. The dramatic decrease in the roughness of substrate **III** compared with substrate **II** emphasizes the effect of annealing, producing large, flat crystalline domains.[12,13] Analysis of the roughness of single grains of substrates **I** and **III** gives similar values, suggesting that the increase in overall roughness in substrate **I** is due to grain boundaries, developing with film thickness.

TEM images of substrates **II** and **III** are shown in Figure 1g,h. The unannealed Au film **II** exhibits small grains (50−100 nm diameter) and substantial roughness, manifested as high image contrast. On the other hand, the annealed film **III** shows a smooth, continuous structure with large, flat grains (200−500 nm diameter). Selected-area electron diffraction of the unannealed film exhibits a diffraction pattern characteristic of a {111} textured, multi-grain structure (Figure 1g, inset), whereas the annealed film (Figure 1h, inset) exhibits a diffraction pattern of a single-crystal (111) Au.

XRD patterns (Figure 2) show intense Au (111) reflections for the three substrates, indicating {111} textured surfaces. The magnified spectra (Figure 2, insets) reveal reflections from the (200), (220), and (311) planes in the unannealed substrate **II**, while the annealed substrates **I** and **III** show an essentially perfect {111} texture, emphasizing again the role of annealing in enhancing crystallinity and uniformity of the films.[12,13]

Transmission UV−vis spectra of substrates **II** and **III** are shown in Figure 3. The average extinction throughout the visible spectrum is 0.5 au, corresponding to 32% transmittance. It should be noted that contributions to the extinction are from

(12) Golan, Y.; Margulis, L.; Rubinstein, I. *Surf. Sci.* **1992**, *264*, 312−326.

(13) Erratum, *Surf. Sci.* **1992**, *273*, 460.

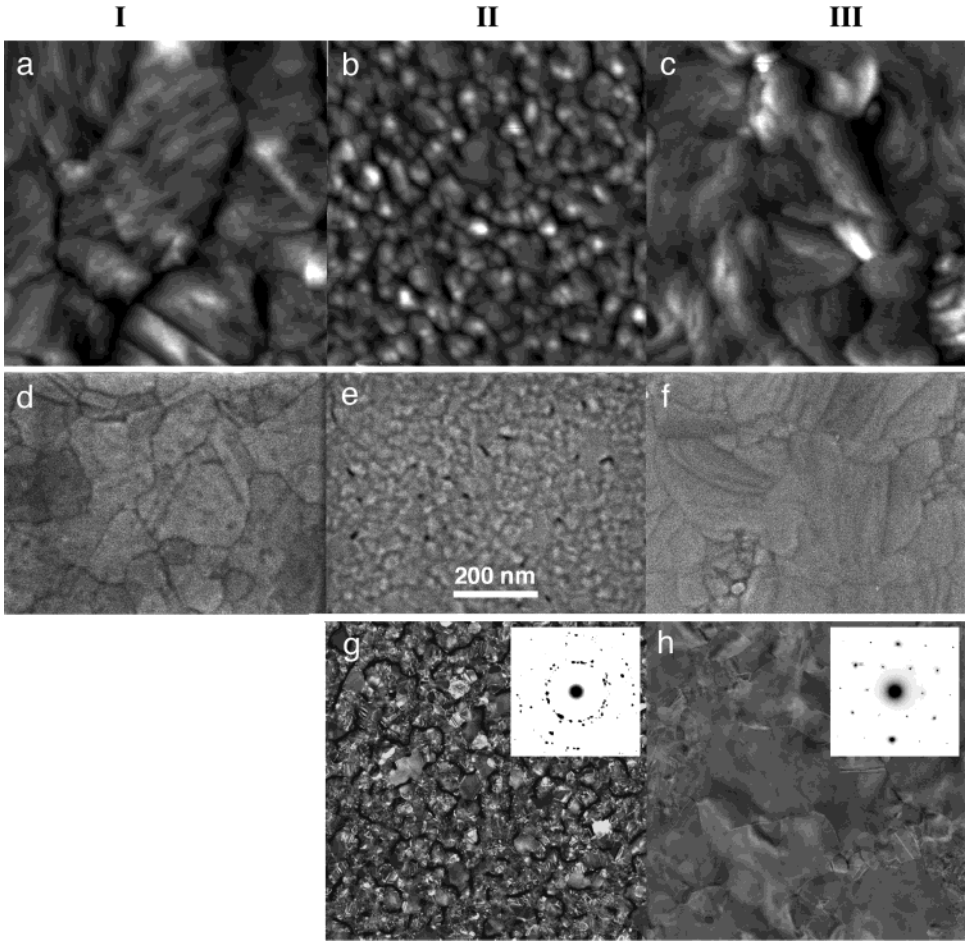

Figure 1. Noncontact AFM (a−c) and HRSEM (d−f) images of Au substrates **I**, **II**, **III**, respectively (**I**: annealed 100 nm Au on amino-silanized Si; **II**: unannealed 15.0 nm Au on amino-silanized glass; **III**: annealed 15.0 nm Au on amino-silanized glass). z-scale: 50 Å (a), 90 Å (b), 35 Å (c). The scale bar corresponds to images a−f. Note that AFM images similar to b and c are obtained when thick (1 mm) glass substrates are used. (g, h) TEM images ($1 \times 1\ \mu m^2$) of Au substrates **II** and **III**, respectively; insets: selected-area (80 nm aperture) diffraction patterns.

both absorption and reflection by the substrate. Spectral changes effected by the annealing include increase in the extinction at longer wavelengths, accompanied by a shift of the absorbance minimum from 529 to 521 nm. Sample-to-sample variability in the spectra of both substrates was ≤ 2.0% (calculated at the wavelength of maximum change).

Cyclic voltammetry (CV) was used for analysis of the Au surface and for determination of the effective surface area (Figure 4). The CV traces show a peak at ca. 0.90 V, typical of oxide formation on a Au (111) surface in H_2SO_4 solution.[14] In agreement with the AFM, HRSEM, TEM, and XRD results, the two annealed substrates **I** and **III** exhibit electrochemical response characteristic of a predominantly Au (111) surface, more pronounced with substrate **III**, while the unannealed substrate **II** shows a typical polycrystalline behavior. The weaker (111) character in the voltammogram of substrate **I** compared with substrate **III** may reflect the influence of the grain boundaries in substrate **I**, as seen in the AFM and HRSEM images (Figure 1). The roughness factor, R_f (defined as the ratio of real to geometric surface area) of the different substrates was determined by integration of the anodic branch (Au oxide formation) of the voltammograms to the Burshtein minimum (see Table 1-S in Supporting Information), using 400 μC/cm^2 as the charge for a 2-electron process on a polycrystalline Au surface.[15] In agreement with the nonelectrochemical measurements described above, substrates **I** and **III** exhibit a similar (within experimental error) roughness factor of 1.33 and 1.39, respectively, while unannealed film **II** shows a significantly higher roughness factor of 1.87.

Underpotential deposition (upd) of Cu on bare Au substrates is sensitive to the surface morphology. The process involves electrodeposition of a monolayer of Cu atoms on the Au surface from a Cu^{2+} solution at potentials positive of the Nernst potential. Cu upd on single-crystal Au (111) occurs in two stages,[16] manifested as two sharp voltammetric peaks for the deposition of 1/3 and 2/3 of a monolayer, while Cu upd on polycrystalline Au[17] shows considerably less defined peaks. While Cu upd on substrate **III** (see Figure 1-S in Supporting Information) exhibits well-defined peaks characteristic of a predominantly Au (111) surface, the upd voltammogram of substrate **II** is typical of polycrystalline Au, in agreement with the results obtained in pure supporting electrolyte (Figure 4). Here, too, the (111) character of the upd voltammogram of

(14) Angerstein-Kozlowska, H.; Conway, B. E.; Hamelin, A.; Stoicoviciu, L. *J. Electroanal. Chem.* **1987**, *228*, 429−453.

(15) Michri, A. A.; Pshenichnikov, A. G.; Burshtein, R. K. *Elektrokhimiya* **1972**, *8*, 364−365.

(16) Magnussen, O. M.; Hotlos, J.; Nichols, R. J.; Kolb, D. M.; Behm, R. J. *Phys. Rev. Lett.* **1990**, *64*, 2929−2932.

(17) Santos, M. C.; Mascaro, L. H.; Machado, S. A. S. *Electrochim. Acta* **1998**, *43*, 2263−2272.

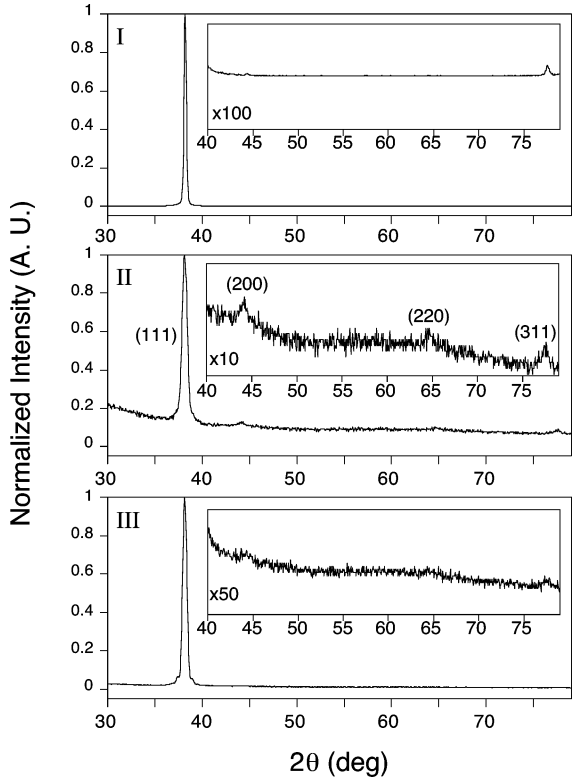

Figure 2. XRD θ-2θ spectra of Au substrates **I**, **II**, **III**. Inset: magnification of the high 2θ range.

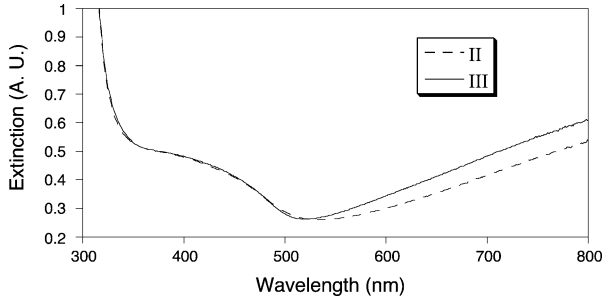

Figure 3. Transmission UV−vis spectra of unannealed (**II**) and annealed (**III**) 15.0 nm Au films on amino-silanized glass (background in air).

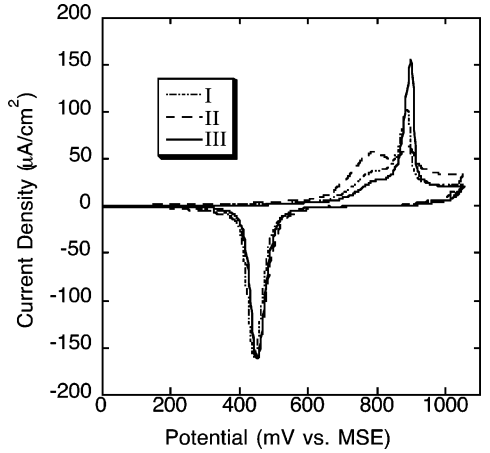

Figure 4. Steady state CV of Au substrates **I**, **II**, **III** in 0.1 M H_2SO_4 showing the Au oxide formation-stripping waves. Scan rate: 0.1 V/s.

substrate **I** is weaker compared with substrate **III**, emphasizing the effect of grain boundaries.

Table 1. Advancing (adv) and Receding (rec) Water Contact Angles (CAs) for Alkanethiol SAMs on the Different Au Substrates[a]

sub-strate	CA adv (st dev), rec (st dev) (deg)		
	$C_8H_{17}SH$	$C_{12}H_{25}SH$	$C_{18}H_{37}SH$
I	104.5 (0.2), 105.1 (0.4)	111.8 (1.0), 109.2 (0.1)	106.7 (0.4), 105.0 (1.7)
II	109.7 (1.6), 108.4 (2.4)	111.2 (2.0), 107.0 (2.6)	109.9 (1.0), 107.8 (0.9)
III	103.1 (0.4), 102.1 (0.7)	106.4 (0.9), 104.1 (0.8)	108.8 (1.3), 107.3 (1.0)

[a] Standard deviation (st dev) values are given in parentheses.

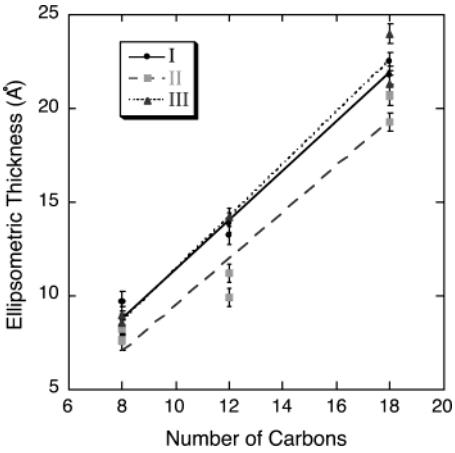

Figure 5. Ellipsometric thicknesses for different chain length alkanethiol SAMs on Au substrates **I**, **II**, **III** (calculated using $n_f = 1.50$, $k_f = 0$).

Self-Assembled Alkanethiol Monolayers. Figure 5 presents ellipsometric thickness results for SAMs of 1-octanethiol ($CH_3(CH_2)_7SH$), 1-dodecanethiol ($CH_3(CH_2)_{11}SH$) and 1-octadecanethiol ($CH_3(CH_2)_{17}SH$) on each of the substrates. The average values of the ellipsometric parameters Δ, Ψ for the bare Au substrates **I**, **II**, **III** were (110.0°, 43.90°), (97.0°, 30.7°), and (101.0°, 32.0°), respectively. Monolayer thicknesses for the annealed substrates **I** and **III** are quite similar and in good agreement with previously reported values,[18,19] whereas the same SAMs on the unannealed substrate **II** exhibit consistently lower ellipsometric thickness. The latter may be the result of somewhat poorer organization of the SAMs on the relatively rough, polycrystalline substrate **II**.

Advancing and receding contact angle (CA) values are summarized in Table 1. In all cases, high advancing CAs and low hystereses are observed, indicating good organization of the monolayers.[18,19] The lower degree of organization of monolayers on substrate **II**, revealed by the ellipsometric results, is not seen in the CA results, emphasizing the different sensitivities of the different techniques. The generally higher CAs on substrate **II** are compatible with the increased roughness of this substrate, as expected for CAs higher than 90°.[20]

FTIR spectroscopy has been used extensively to characterize organic mono- and multilayers on Au surfaces, usually in the reflection−absorption mode at grazing incidence (typically 80°), using thick (100−200 nm) Au films to obtain effective reflection. As shown here, 15-nm-thick Au on glass provides sufficient reflectivity for RA-FTIR spectroscopy of SAMs. Note that RA-FTIR spectra of 15-nm-thick Au on the thin glass substrates (0.3 mm thick) show interference fringes at >2000 cm^{-1}, while the use of the thick glass substrates (1 mm thick)

(18) Bain, C. D.; Whitesides, G. M. *J. Am. Chem. Soc.* **1989**, *111*, 321−335.
(19) Ron, H.; Rubinstein, I. *J. Am. Chem. Soc.* **1998**, *120*, 13 444−13 452.
(20) Wenzel, R. N. *Ind. Eng. Chem.* **1936**, *28*, 988−994.

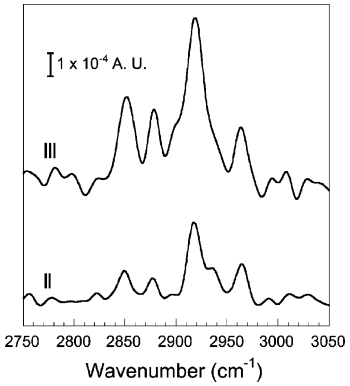

Figure 6. RA-FTIR spectra of octadecanethiol SAMs on unannealed (**II**) and annealed (**III**) Au substrates prepared on 1 mm thick microscope slides.

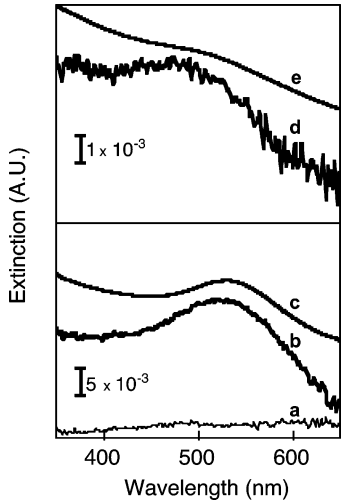

Figure 7. Absorbance spectra for (a) 1,10-decanedithiol SAM on substrate **III**; (b) TOAB-capped NP layer on the SAM in a; (c) TOAB-capped NP solution in toluene; (d) octanethiol-capped NP layer on the SAM in a; (e) octanethiol-capped NP solution in $CHCl_3$.

Table 2. IR Vibrational Frequencies for Octadecanethiol SAMs on Substrates II and III

	ν (cm^{-1})			
substrate	-$CH_{3\ asym}$	-$CH_{2\ asym}$	-$CH_{3\ sym}$	-$CH_{2\ sym}$
II	2964	2917	2878	2850
III	2963	2918	2879	2851
literature values[21,22]	2964	2919	2878	2850

eliminates this problem. Figure 6 presents RA-FTIR spectra of octadecanethiol SAMs on substrates **II** and **III**, prepared on the thick glass substrates. The spectra on both substrates are characteristic of well-ordered SAMs, in good agreement with literature results,[21,22] as also summarized in Table 2.

Binding of Au Nanoparticles (NPs) to Annealed, Transparent Au Substrates. Figure 7 shows UV−vis spectra for the binding of TOAB-capped and octanethiol-capped Au NPs to transparent Au substrate **III**. In both cases, a prominent surface plasmon absorbance is observed for the NPs on the surface, indicating successful NP binding to the surface. The ellipsometric and CA results (Table 3) are consistent with binding of the different types of NPs to the surface. AFM images of the substrates following NP binding are shown in Figure 8. The NP layers are clearly imaged in both cases. The Au substrate grain structure is seen under the octanethiol-capped NPs (Figure 8b), probably due to the lower density and thickness of this NP layer. The latter is attributed to the difference in binding kinetics, being faster for TOAB-capped NPs.

Table 3. Ellipsometry and Water Contact Angle (CA) Results for Nanoparticle (NP) Monolayers Bound to 1,10-decanedithiol SAMs on Substrate III

	NPs on dithiol SAM	
adsorbate	ellipsometry[a] -$\delta\Delta$ (deg)	CA (deg) adv(st dev), rec(st dev)
TOAB-capped NPs	8.1 ± 0.3	86 (3), 36 (4)
octanethiol-capped NPs	3.0 ± 0.1	105 (2), 96 (4)

[a] For the SAM of 1,10-decanedithiol, $-\delta\Delta = 1.1° \pm 0.1°$.

Binding of Protoporphyrin IX (PPIX) to SAMs of 11-Mercaptoundecanoic Acid (MUA). To demonstrate comprehensive characterization of a chromophore monolayer, PPIX was bound to preformed monolayers of MUA on the different Au substrates, either with (**A**) or without (**B**) binding of Cu^{2+} to the MUA monolayer (Scheme 1). Binding of Cu^{2+} to carboxylate-functionalized SAMs for multilayer construction was previously reported.[23]

Ellipsometry and CA results for the stepwise assembly of PPIX are given in Table 4. The ellipsometric thicknesses of MUA SAMs on all the substrates are similar and in agreement with previously reported data.[18] For PPIX on Cu^{2+}-bound MUA (**B**) a reproducible film thickness of ca. 35 Å is obtained. This result is consistent with the estimated value of ca. 14 Å for a fully extended, perpendicular protoporphyrin molecule,[24] where the small difference may be explained by a certain change in the film refractive index upon Cu^{2+} binding. In contrast, PPIX bound directly to MUA (**A**) shows smaller (ca. 28 Å) and quite irregular ellipsometric thickness values, suggesting disorder and a lower coverage.

The CAs for MUA and Cu^{2+}-bound MUA SAMs (Table 4) are low, indicating, as expected, nearly complete wetting. Self-assembly of PPIX onto the Cu^{2+}-treated SAM (**B**), producing a hydrophobic (vinyl- and methyl-terminated) surface, resulted in much higher CAs (ca. 75°) with a relatively low hysteresis. Applying the same process without Cu^{2+} binding (**A**) resulted in much lower CAs (ca. 50°) with a large hysteresis, suggesting again poor organization and low coverage.

Transmission UV−vis spectroscopy results for the formation of a PPIX SAM on substrate **III** are shown in Figure 9. PPIX in solution shows a characteristic Soret band at 403 nm and a weaker Q-band absorbance in the region 480−650 nm. The transmission spectrum of sample **B** (binding to the carboxylate/Cu^{2+} SAM) shows an intensity of 0.012 ± 0.001 au, consistent with previous results for porphyrin monolayers.[25] The Soret band of PPIX in the SAM is broader and blue-shifted by ca. 17 nm compared with that of PPIX in solution (Figure 9). The shift may be indicative of cofacial interaction of porphyrin rings in

(21) Laibinis, P. E.; Whitesides, G. M.; Allara, D. L.; Tao, Y. T.; Parikh, A. N.; Nuzzo, R. G. *J. Am. Chem. Soc.* **1991**, *113*, 7152−7167.
(22) Ron, H.; Cohen, H.; Matlis, S.; Rappaport, M.; Rubinstein, I. *J. Phys. Chem. B* **1998**, *102*, 9861−9869.
(23) Evans, S. D.; Ulman, A.; Goppert-Beranducci, K. E.; Gerenser, L. J. *J. Am. Chem. Soc.* **1991**, *113*, 5866−5868.
(24) The height of a PPIX molecule was estimated with CS Chemdraw and ChemBats3D software using MM2 energy-minimization (CambridgeSoft Corp., USA).
(25) Kalyuzhny, G.; Vaskevich, A.; Ashkenasy, G.; Shanzer, A.; Rubinstein, I. *J. Phys. Chem. B* **2000**, *104*, 8238−8244.

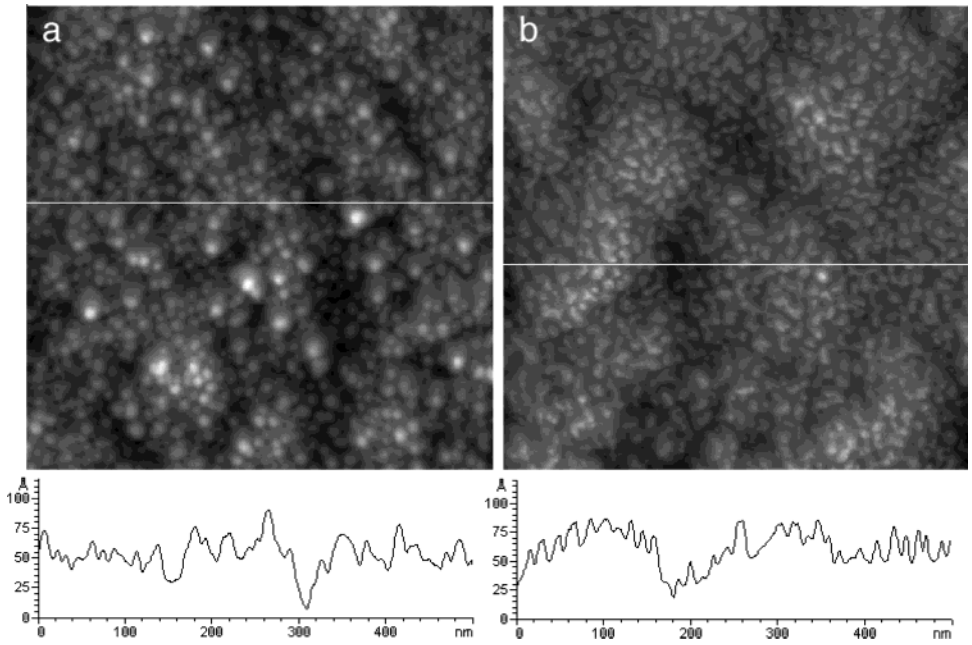

Figure 8. Noncontact AFM images (500 × 500 nm^2) of (a) TOAB-capped and (b) octanethiol-capped NP monolayers bound onto 1,10-decanedithiol SAMs on substrate **III**.

Table 4. Ellipsometric Thickness and Contact Angle (CA) Data for the Stepwise Binding of PPIX to a Monolayer of MUA, Either Untreated (Route A) or Treated (Route B) with Cu^{2+} as In Scheme 1 (hyphen indicates complete wetting)

	MUA		Cu^{2+}		PPIX	
route (substrate)	thickness (±1 Å)	CA (deg) adv (st dev), rec (st dev)	thickness (±1 Å)	CA (deg) adv (st dev), rec (st dev)	thickness (±1 Å)	CA (deg) adv (st dev), rec (st dev)
A (I)	16.6	18.2 (1.9), -			29.7	50.0 (7.0), 29.8 (2.9)
A (II)	15.4	19.3 (2.8), -			25.1	47.2 (4.9), 22.7 (2.9)
A (III)	16.3	21.7 (2.4), -			30.8	52.9 (4.7), 23.1 (3.0)
B (I)	18.2	31.4 (4.6), -	18.7	35.0 (1.5), 32.0 (4.8)	36.0	76.1 (1.0), 66.2 (3.7)
B (II)	14.5	17.0 (2.5), -	18.4	31.6 (3.6), 25.0 (3.6)	34.1	75.9 (0.9), 72.0 (2.9)
B (III)	17.2	21.0 (1.8), -	19.5	35.4 (2.9), 26.7 (1.9)	34.1	78.6 (0.5), 73.5 (2.0)

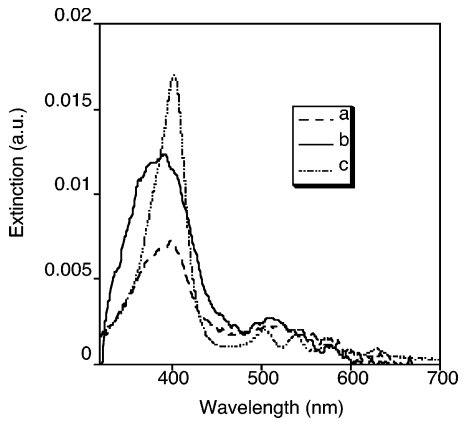

Figure 9. Transmission UV−vis spectra of substrate **III** after binding of PPIX to SAMs of MUA (a) and MUA/Cu^{2+} (b). (c) is a spectrum of a PPIX solution in ethanol.

the monolayer, as previously observed with an analogous molecule in solution[26] and attributed to cofacial dimerization. Practically no change in the spectrum of sample B was observed upon immersion in ethanol, indicating low solvent dependence of the interaction. The transmission spectrum of sample **A** (direct binding to the carboxylate SAM) shows a much weaker Soret band compared with **B** (about half the intensity) with no significant shift (Figure 9), suggesting again a lower coverage and poor organization of the porphyrin molecules.

(26) Dairou, J.; Vever-Bizet, C.; Brault, D. *Photochem. Photobiol.* **2002**, *75*, 229−236.

Table 5. XPS Atomic Concentrations at Two Takeoff Angles (Φ) for Sample B (Scheme 1) on Substrates I and III

substrate, Φ (deg)	atomic concentration					
	Cu	N	S	C	O	Au
I, 90°	1.4	3.2	1.4	55.4	10.4	28.2
I, 25°	1.3	4.6	1.5	64.3	11.7	16.7
III, 90°	2.2	3.1	1.4	52.8	15.3	25.3
III, 25°	2.1	3.9	0.8	61.7	17.8	13.8

XPS analysis, including angle-resolved measurements, was carried out on samples prepared as in Scheme 1**B** on the annealed substrates **I** and **III**. The results, summarized in Table 5, show a higher atomic concentration ratio of N/S for substrate **III** compared with substrate **I,** suggesting higher coverage of PPIX molecules on the MUA-modified substrate **III**. For both substrates the ratios of Cu/N and S/N decrease at lower takeoff angles, confirming the higher position of the N atoms (i.e., the porphyrin), as illustrated in Scheme 1. This result also rules out possible metalation of the porphyrin with Cu^{2+} ions during the process. The XPS data therefore confirm that PPIX binding in sample **B** is mediated by Cu^{2+} ion binding to carboxylate groups (as in Scheme 1).

It should be noted that a carboxylate/Cu^{2+} type multilayer construction was previously reported with carboxylate-functionalized Au nanoparticles,[27] but an attempt to use this scheme on flat surfaces (for binding arachidic acid to a SAM of MUA preloaded with Cu^{2+} ions) was unsuccessful.[23] The binding of PPIX reported here may be promoted by the presence of two carboxylate groups on PPIX, as well as stacking interaction between porphyrins in the layer.

Conclusions

Semi-transparent, continuous, 15-nm-thick Au films evaporated at 0.5 Å/sec on silanized glass and annealed were shown to provide stable, morphologically well-defined and highly versatile substrates for the preparation and study of SAMs and other kinds of ultrathin overlayers on Au. Such substrates, in the thickness range from 15 to 20 nm, represent an optimal situation with respect to the Au film thickness, being at the same time semi-transparent, reflective, and electrically conductive. This enables, as demonstrated here, the use of an exceedingly wide spectrum of characterization methods, applied to the same substrate, including AFM, XRD, TEM, SEM, XPS, electrochemical methods, CA measurements, ellipsometry, transmission spectroscopy, and RA-FTIR spectroscopy. Note that an Au film thickness of 15 nm is also compatible with surface plasmon resonance (SPR) measurements[28] (not shown here). These substrates exhibit a morphology similar to that of thick ($\geq$100 nm) annealed Au films, showing large, flat domains, a strong {111} texture and a low roughness factor. The thin, transparent, conductive Au substrates can, therefore, replace the widely used 100−300 nm evaporated Au films, while adding experimental capabilities and being considerably more economical. Note that replacing the silanized glass substrates with silanized quartz would expand the spectroscopic capabilities to include the UV range, enabling, for example, optical monitoring of DNA binding to Au.

The usefulness of the annealed, transparent Au films in the study of ultrathin films on Au was manifested with several different systems. Cu underpotential deposition (upd) demonstrated electrochemical analysis of the surface morphology. Alkanethiol SAMs prepared on such substrates show ellipsometric thickness, contact angles and FTIR spectra similar to those measured with thick, annealed Au films. Binding of Au nanoparticle layers was used to demonstrate the suitability of such substrates to scanning probe analysis and transmission spectroscopy.

Binding of protoporphyrin IX (PPIX) to a carboxylate-terminated SAM on such substrates was used to demonstrate a comprehensive study of chromophore layers on Au. PPIX adsorbed onto a SAM of 11-mercaptoundecanoic acid (MUA) shows superior organization when Cu^{2+} ions are used for binding between PPIX and MUA. Ellipsometry, XPS, transmission UV−vis spectroscopy, and CA data support a model in which binding occurs through the carboxylate groups (Scheme 1). In contrast, adsorption of PPIX onto a MUA SAM without intermediate Cu^{2+} binding resulted in poor, disordered layers.

Acknowledgment. Support from the Israel Science Foundation and the Minerva Foundation, Munich, is gratefully acknowledged. M.W. is recipient of the Levy Eshkol Scholarship, Israel Ministry of Science. A.V. acknowledges support from the Kamea Program, Israel Ministry of Absorption. We thank Dr. E. Wachtel for assistance with the XRD experiments, Dr. Z. Barkay (Tel-Aviv University) for the HRSEM images, Dr. I. Ruach-Nir for assistance with the TEM experiments, and Dr. H. Cohen for the XPS measurements.

Supporting Information Available: (i) Roughness of the Au substrates, determined from cyclic voltammetry; (ii) Cu upd voltammograms for the Au substrates. This material is available free of charge via the Internet at http://pubs.acs.org.

JA0396448

(27) Zamborini, F. P.; Hicks, J. F.; Murray, R. W. *J. Am. Chem. Soc*. **2000**, *122*, 4514−4515.
(28) Ikehata, A.; Li, X.; Itoh, T.; Ozaki, Y.; Jiang, J.-H. *App. Phys. Lett*. **2003**, *83*, 2232−2234.